

Multi-Modal Scene Graph with Kolmogorov–Arnold Experts for Audio-Visual Question Answering

Zijian Fu* Changsheng Lv* Mengshi Qi[†] Huadong Ma
 State Key Laboratory of Networking and Switching Technology,
 Beijing University of Posts and Telecommunications, China
 {zijianfu, lvchangsheng, qms, mhd}@bupt.edu.cn

Abstract

In this paper, we propose a novel Multi-Modal Scene Graph with Kolmogorov–Arnold Expert Network for Audio-Visual Question Answering (SHRIKE). The task aims to mimic human reasoning by extracting and fusing information from audio-visual scenes, with the main challenge being the identification of question-relevant cues from the complex audio-visual content. Existing methods fail to capture the structural information within video, and suffer from insufficient fine-grained modeling of multi-modal features. To address these issues, we are the first to introduce a new multi-modal scene graph that explicitly models the objects and their relationship as a visually grounded, structured representation of the audio-visual scene. Furthermore, we design a Kolmogorov–Arnold Network (KAN)-based Mixture of Experts (MoE) to enhance the expressive power of the temporal integration stage. This enables more fine-grained modeling of cross-modal interactions within the question-aware fused audio-visual representation, leading to capture richer and more nuanced patterns and then improve temporal reasoning performance. We evaluate the model on the established MUSIC-AVQA and MUSIC-AVQA v2 benchmarks, where it achieves state-of-the-art performance. Code and model checkpoints will be publicly released.

1. Introduction

Audio-Visual Question Answering (AVQA) aims at answering questions by simulating the human ability to interpret audiovisual scenes by capturing useful auditory and visual cues. This form of multimodal reasoning remains a significant challenge for machine intelligence, yet it is essential for applications such as robot navigation [55], embodied intelligence [38, 43, 53], autonomous driving [11, 36, 57, 60] and video surveillance [12, 41], as well as video retrieval

*Equal contribution

[†]Corresponding author

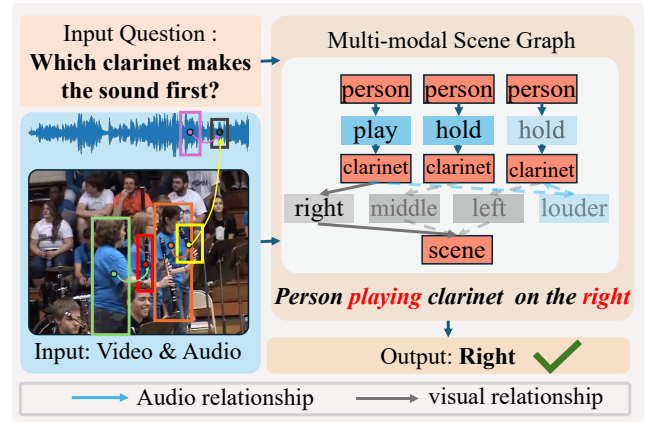


Figure 1. Illustration of AVQA task. Given an video, we construct a multi-modal scene graph that encodes objects, visual and audio relationships. The question text is then used to select the most relevant relationships, forming a question-conditioned subgraph that is fed into the fusion and reasoning module to output the answer.

and summarization [10].

Most of existing methods in AVQA were introduced to address challenges like spatio-temporal grounding [19, 27], cross-modal adaptation of pre-trained visual backbones [9, 32, 53], and question-guided temporal segment selection [6, 37], yet often overlook visual structural information, particularly when overlapping audio cues make it too hard to distinguish individual sounds. For example, as shown in Figure 1, answering the question “Which clarinet makes the sound first?” based solely on audio can be ambiguous due to sound blending. In contrast, learning from multimodal structural relationships, such as spatial arrangement, can provide clearer cues for accurate identification. Therefore, we are the first to extend the current scene graph [21] into the multi-modal field (*i.e.*, image, text and audio) to explicitly model audio-visual structural relationships, incorporating structural context as complementary information to enhance overall audio-visual understanding.

Furthermore, another key challenge lies in the tempo-

ral grounding of question-relevant cues. Existing methods [24] adopt a Mixture-of-Experts (MoE) [49] framework with MLP-based experts to capture temporal dependencies through adaptive weighting. While such MLP-based experts are effective at modeling coarse global temporal trends, the learned temporal weights remain implicit and predominantly coarse-grained, making them insufficient for aggregating fine-grained, question-relevant cross-modal cues. Kolmogorov-Arnold Networks (KANs) [1], as a novel neural network architecture, have gained significant attention in the deep learning community due to their strong data-fitting capabilities. Compared to MLPs, KANs exhibit stronger locality under the same network depth, owing to their spline-based parameterization. This locality allows the temporal integration module to more easily focus on question-relevant events, enabling finer-grained modeling of cross-modal temporal patterns and ultimately improving temporal reasoning performance. To the best of our knowledge, we are the first to explore KAN-based experts for audio-visual question answering.

In this paper, we propose a new Multi-Modal Scene GRaph wIth Kolmogorov-Arnold framework for Audio-Visual QuEstion Answering, termed as **SHRIKE**. First, features are extracted from the input video, audio, and questions using their respective encoders. Next, we introduce a new **Multi-Modal Scene Graph Decoder (M^2SG)**, which generates triplet features representing structural information in each frame based on its audio and visual features. These features are further fused with the temporally grounded visual and audio features via the cross-attention mechanism, serving as enhanced audio cues and complementary structural context. Finally, a classifier is employed to predict the answer to the question. Meanwhile, within the MoE framework, we introduce a new **Kolmogorov-Arnold Network (KAN) based Expert Module** to enhance the expressive power of temporal integration. Specifically, KAN is employed to replace the multilayer perceptron (MLP) within the feed-forward networks (FFNs) that constitute the diverse experts in the MoE. By concentrating multiple Gaussian distributions along the temporal axis, KAN learns and adaptively aggregates the weights of these distributions, generating a soft mask that facilitates the extraction of sharper and more reliable temporal dependencies.

Our main contributions can be summarized as follows:

(1) We propose a novel Multi-Modal Scene Graph framework (*i.e.*, SHRIKE), integrated with the Kolmogorov-Arnold Network (KAN) for Audio-Visual Question Answering, which enhances reasoning capabilities through the newly designed Multi-Modal Scene Graph Decoder, particularly in scenarios with overlapping and hard-to-distinguish audio cues.

(2) We introduce a new KAN-based expert module in the MoE framework, replacing MLPs with spline-based KAN

experts to enhance the expressive power of the temporal integration and reasoning performance.

(3) Experimental results show our proposed SHRIKE achieves state-of-the-art performance on the MUSIC-AVQA and MUSIC-AVQA 2.0 datasets, while providing explicit temporal grounding of audio and visual cues.

2. Related Work

Audio-Visual Scene Understanding. Inspired by human multisensory perception, research has increasingly focused on audio-visual scene understanding, spanning tasks like action recognition [13, 23], question answering [2], object localization [17], and segmentation [59]. Recent studies have advanced audio-visual question answering by enhancing efficiency and reasoning capabilities. LAVISH [32] introduced adapter-based architectures, enabling generalization from visual to audio-visual scenarios with minimal additional parameters. COCA [25] and M2KVDG [33] utilized causal graphs to improve multi-modal interaction and reasoning. Unlike these approaches, our method integrates graph structured audio-visual information to further enhance model reasoning.

Scene Graph (SG). SG was originally introduced for image retrieval [7, 21, 39, 40, 42] by decomposing an image into objects and their relations, and have since benefited visual retrieval [58], visual question answering [44], and captioning [30]. WhereAmI [5] enables 3D scene retrieval from natural language, while XNMs [50] achieve high accuracy on CLEVR [22] via structured reasoning. However, these approaches are confined to purely visual settings and ignore audio-visual relevance. In contrast, we are the first to integrate multi-modal scene graphs into AVQA, improving reasoning especially when audio cues are ambiguous.

Kolmogorov-Arnold Networks (KANs). According to the Kolmogorov-Arnold theorem [1], enabling multivariate functions to be expressed via univariate functions and additions, has inspired neural network designs like KANs. KANs replace linear weights with learnable splines, reducing parameters and enhancing generalization [35]. Extensions include TimeKAN for frequency decomposition [18] and PowerMLP, which matches MLP speed while surpassing KANs in expressiveness [45]. To the best of our knowledge, we are the first to leverage KANs to enhance the expressive power of temporal integration in modeling complex cross-modal temporal dependencies for AVQA.

3. Method

3.1. Overview

As shown in Figure 2, our proposed SHRIKE is designed to advance audio-visual question answering by (i) constructing an explicit multi-modal scene graph that provides structured entity-relation cues, and (ii) introducing a KAN-

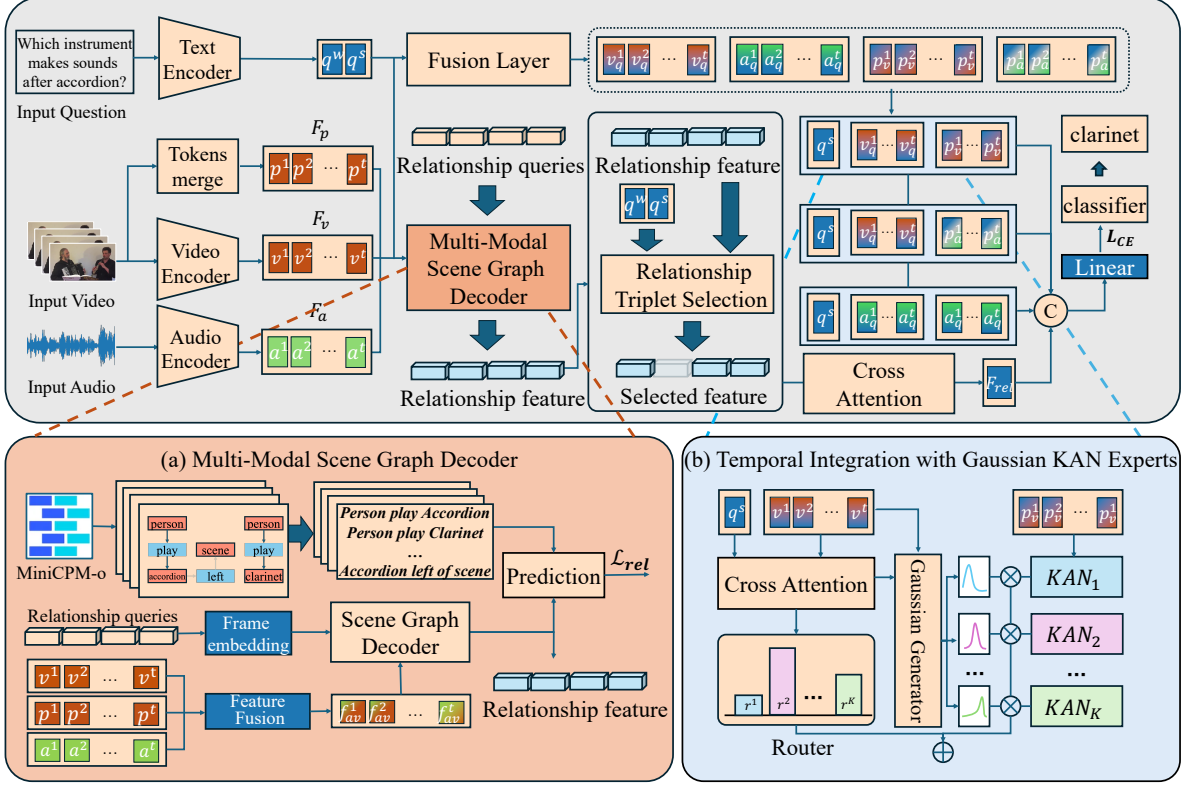


Figure 2. Overview of the proposed SHRIKE: Features from each modality are obtained by passing the input through a corresponding pretrained encoder. Then we propose (a) Multi-Modal Scene Graph Decoder to extract scene graph features from the video and select specific triplets using the relationship triplets selection. Through (b) Temporal Integration with Gaussian KAN Experts, our model achieves effective question-guided localization of critical temporal segments, enhancing temporal reasoning and multi-modal understanding.

based expert module that enhances temporal integration of audio and visual evidence. Our model is optimized in a two-stage manner. In the first stage, the Multi-Modal Scene Graph Decoder is trained; while in the second stage, this decoder is frozen, and the remaining components of the model are trained conditioned on the predicted scene graphs.

Problem Formulation. Given an input data represented as $\langle \mathcal{V}, \mathcal{A}, q_s \rangle$, where \mathcal{V} denotes the video, \mathcal{A} denotes the audio, and q_s represents the question. The output is a predicted answer y_c , which belongs to a predefined set of candidate answers \mathcal{C} denoted as $y_c \in \mathcal{C}$.

Multi-Modal Scene Graph Definition. Inspired by [21], we define a multi-modal scene graph denoted by \mathcal{G} . Let $\mathcal{G} = (\mathcal{O}, \mathcal{R})$, where \mathcal{O} represents the set of all entities in the dataset and $\mathcal{R} = [\mathcal{R}^a, \mathcal{R}^v]$ represents the set of all relationships between the entities, \mathcal{R}^a denotes the set of audio-related relationships and \mathcal{R}^v denotes the set of visual-related relationships. Unlike the traditional scene graphs [21], these relationships not only include spatial relations but also audio-related interactions (e.g., louder than). Specifically, given an input video \mathcal{V} , our goal is to construct a scene graph $g_t = (o_t, r_t)$ for each time segment t in the video, where $o_t \in \mathcal{O}$ represents the entities

set, $r_t = [r_t^a, r_t^v]$, $r_t^v \in \mathcal{R}^v$ and $r_t^a \in \mathcal{R}^a$ represents the relationships set within the corresponding frame. The multi-modal scene graph for the entire video is represented by the set of graphs $\mathcal{G} = \{g_t\}_{t=1}^T$. For each time segment t , we propose to predict the set of relationship triplets r_t that can be described as $\langle \text{subject}, \text{predicate}, \text{object} \rangle$, and denoted by $r_t = \{r_{t,i}\}_{i=1}^N$ in each video frame where N is the number of triplets in segment t . Our model is directed to produce structured outputs in the form of triplets $r_i = \langle \text{subject}, \text{predicate}, \text{object} \rangle$, constrained by the predefined sets \mathcal{O} and \mathcal{R} . These triplets are then organized into $g_t = (o_t, r_t)$, where o_t represents all subjects and objects appearing in the segment.

Multi-Modal Scene Graph Annotations. We first define a vocabulary of entities \mathcal{O} and relations \mathcal{R} . Then, for each temporal segment t , we feed the corresponding audio-visual clip into MiniCPM-o [56], prompting it to output relation triplets $r_i = \langle \text{subject}, \text{predicate}, \text{object} \rangle$ constrained by \mathcal{O} and \mathcal{R} . The resulting triplets are assembled into a scene graph $g_t = (o_t, r_t)$, where o_t denotes the set of subjects and objects in segment t . Finally, we collect all segment-level graphs into the annotation set $\mathcal{G} = \{g_t\}_{t=1}^T$.

Implementation details and prompts are provided in the supplementary material.

Input Representations. Given a video \mathcal{V} and its corresponding audio \mathcal{A} , we follow [24] and employ pre-trained audio, visual, and text encoders with frozen parameters to extract features. For each segment t : **(1) Audio.** We use the pre-trained VGGish model [15] to obtain audio features $a_t \in \mathbb{R}^D$, forming $F_a = \{a_t\}_{t=1}^T \in \mathbb{R}^{T \times D}$. **(2) Visual.** A pre-trained CLIP visual encoder [46] is used to extract frame-level features $F_v = \{v_t\}_{t=1}^T \in \mathbb{R}^{T \times D}$ from the [CLS] token, and patch-level features $F_p = \{p_t\}_{t=1}^T \in \mathbb{R}^{T \times M \times D}$ via Token Merging [3], where M is the number of visual tokens. **(3) Text.** The input question is tokenized and passed through the CLIP text encoder to obtain a sentence-level feature $q_s \in \mathbb{R}^D$ from the [EOT] token and word-level features $q_w \in \mathbb{R}^{M' \times D}$, where M' denotes the token number.

3.2. Multi-Modal Scene Graph Generation

In this section, we introduce the fusion of audio and visual features, along with the newly designed Scene Graph Decoder for triplet extraction in the scene graph, and present the process of relationship triplet selection.

Feature Fusion. To comprehensively capture all potential relationships within the scene graph, we intentionally exclude question-related textual features from the model input and instead focus solely on fusing visual and auditory modalities. Incorporating textual information may introduce bias or unintended priors that could interfere with accurate scene graph prediction. Specifically, we employ cross-attention (CA) and self-attention (SA) mechanisms to fuse visual features F_v and audio features F_a as follows:

$$F'_v = F_v + \text{SA}(F_v) + \text{CA}(F_v | F_a), \quad (1)$$

$$F'_a = F_a + \text{SA}(F_a) + \text{CA}(F_a | F_v), \quad (2)$$

where CA and SA denote cross-attention and self-attention, respectively. The tensors $F'_v, F'_a \in \mathbb{R}^{T \times D}$ represent the enhanced visual and audio features. To achieve finer spatial granularity and detailed object property identification, we concatenate F'_v and F'_a , and apply cross-attention using the concatenated feature as the query and patch-level visual features F_p as the key and value, formulated as:

$$F_{av} = \text{CA}(\text{Concat}(F'_v, F'_a) | F_p), \quad (3)$$

where $F_{av} \in \mathbb{R}^{T \times D}$ represents the fused feature, and Concat denotes the concatenation operation.

Scene Graph Decoder. We initialize learnable relationship queries $Q \in \mathbb{R}^{T \times L \times D}$, where T , L , and D denote the number of frames, queries, and hidden dimension size, respectively. Inspired by Frame Embedding [52], we augment the queries with positional encodings to encode temporal information. These queries serve as the input to a three-layer

Transformer decoder, where the fused audiovisual features F_{av} are used as keys and values. For the l -th layer:

$$Q^{(l+1)} = \text{TransformerDecoderLayer}(Q^{(l)}, F_{av}), \quad (4)$$

Then we can achieve the final layer output, denoted as $F_{rel} = Q^{final} \in \mathbb{R}^{T \times L \times D}$, represents triplet relationship features in the audiovisual scene. During training, these features are then passed through a prediction head implemented as a two-layer feed-forward network (FFN) with a GELU activation function.

Relationship Triplet Selection. The scene contains multiple triplets, but not all of them are relevant to the given question. To address this, we introduce a Relationship Triplet Selection strategy to identify the most relevant triplets. Specifically, for each time segment t , we compute the attention weights between the question feature q_s and the relationship triplet features F_{rel}^t using scaled dot-product attention. The segments with the highest attention weights, along with their corresponding indices, are then selected:

$$W_{rel} = \text{softmax} \left(\frac{q_s F_{rel}^t{}^\top}{\sqrt{D}} \right), \quad (5)$$

$$F_{top_k}^t = \phi_{QTP}(F_{rel}^t, W_{rel}, top_k), \quad (6)$$

where $W_{rel} \in \mathbb{R}^{1 \times N}$ represents the attention weights, and D is the dimension of q_s . The selection operation is denoted as ϕ_{QTP} , and the resulting top- k features are represented as $F_{top_k}^t \in \mathbb{R}^{top_k \times D}$.

3.3. Fusion Layer

Subsequently, we integrate information from the video, audio, and text modalities. Specifically, we use self-attention to enhance intra-modal relationships, and then apply cross-attention with the other two modalities to achieve inter-modal fusion: visual features F_v are used as queries, while audio features F_a serve as keys and values. We employ word-level question features q_w as keys and values. Audio features F_a are processed in the similar manner. Finally, the resulting features are combined with the original input via a residual connection, as follows:

$$v_q = F_v + \text{SA}(F_v) + \text{CA}(F_v | F_a) + \text{CA}(F_v | q_w), \quad (7)$$

$$a_q = F_a + \text{SA}(F_a) + \text{CA}(F_a | F_v) + \text{CA}(F_a | q_w), \quad (8)$$

where $v_q = \{v_q^t\}_{t=1}^T \in \mathbb{R}^{T \times D}$ and $a_q = \{a_q^t\}_{t=1}^T \in \mathbb{R}^{T \times D}$. Afterwards, the patch-level visual features F_p are aligned within the context to enhance semantic consistency. The process can be described as follows:

$$F'_p = F_p + \text{SA}(F_p), \quad (9)$$

$$p_v = \text{CA}(v_q | F'_p), p_a = \text{CA}(a_q | F'_p), \quad (10)$$

where $p_v = \{p_v^t\}_{t=1}^T \in \mathbb{R}^{T \times D}$ and $p_a = \{p_a^t\}_{t=1}^T \in \mathbb{R}^{T \times D}$. Thus we obtain the audio and visual modalities enriched with contextual information from the question.

3.4. Gaussian KAN-based Experts

Inspired by the success of LLM [8, 26], we adopt the Mixture of Experts (MoE) [49] framework in our model, by leveraging a Gaussian distribution to model temporal patterns. To enhance the expressive power of temporal integration, we are first to leverage the Kolmogorov-Arnold Network (KAN) as the expert network in our model.

Gaussian Generator. In order to distribute the Gaussian centers of multiple expert models across the temporal dimension, we adopt the cross-attention to align the question features q_s with the fused multimodal features v_q in Section 3.3. The resulting features v'_q are then projected through a fully connected layer (FC) to map the input dimension D to a 2-dimensional output, yielding the mean (μ) and standard deviation (σ) of the Gaussian distribution, formalized as follows:

$$v'_q = \text{CA}(q_s | v_q), \mu_v, \sigma_v = \text{FC}(v'_q), g = \mathcal{N}(\mu_v, \sigma_v^2), \quad (11)$$

Integrating Temporal Information. We employ Kolmogorov-Arnold Networks (KAN) to replace MLPs within each expert, aiming to enhance the expressive power of temporal integration. Let $\mathcal{F}_{\text{KAN}}(x)$ denote the output of the KAN transformation applied to the input d -dimensional features $x = [x_1, x_2, \dots, x_d]$, which can be defined as:

$$\mathcal{F}_{\text{KAN}}(x_i) = \sum_{i=1}^d \left(\sum_{k=1}^K c_{ijk} B_k(x_i) \right), \quad (12)$$

where x_i represents the i -th dimension, $B_k(x_i)$ denotes the k -th basis function (*i.e.*, B-spline) applied to x_i , and c_{ijk} is the learnable coefficient in the KAN. To capture temporally critical segments, we adopt a Mixture of Experts (MoE) framework [24]. For each KAN-based expert, we design multiple Gaussian distributions $\{g^i\}_{i=1}^E$ using Gaussian Generators, where E denotes the number of experts. For features $o \in \{a, p_a, p_v\}$, where p_a and p_v are from Equation (10), the procedure is formulated as follows:

$$\widetilde{F}_o = \sum_{i=1}^E g_o^i r_o^i \mathcal{F}_{\text{KAN}}(x_o^i), \text{ where } r_o = \text{FC}(v'_q), \quad (13)$$

Here, $\{g_o^i\}_{i=1}^E \in g_o$ represents the Gaussian distributions corresponding to feature o , and $\{r_o^i\}_{i=1}^E$ denotes the routing scores for feature o , obtained via a fully connected layer mapping from feature dimension D to the number of experts E . Finally, we obtain the MoE-aggregated features, *i.e.*, \widetilde{F}_a , \widetilde{F}_{p_a} , and \widetilde{F}_{p_v} .

3.5. Optimization

Our proposed SHRIKE framework incorporates two loss functions: **(1) Task-specific Classification Loss** $\mathcal{L}_{\text{task}}$ for

the Audio-Visual Question Answering task. We concatenate the MoE-aggregated features \widetilde{F}_a , \widetilde{F}_{p_a} , and \widetilde{F}_{p_v} with relationship features along the feature dimension and pass them through a fully connected layer to construct a classifier, yielding the predicted answer \hat{y}_c . **(2) Relationship Prediction Loss** \mathcal{L}_{rel} from the Scene Graph Decoder in Section 3.2. We employ a Hungarian loss $\mathcal{L}_{\text{match}}$ [4] to optimally match the predicted relationship triplet $\hat{r}_{t,i}$ with the ground-truth labels $r_{t,i}$ from the Multi-Modal Scene Graph Annotations generated by miniCPM-o [16]. This can be expressed as:

$$\hat{\sigma}_{\text{rel}} = \arg \min_{\sigma \in \mathfrak{S}_N} \sum_{t=1}^T \sum_{i=1}^N \mathcal{L}_{\text{match}}(y_i^t, \hat{y}_{\sigma(i)}^t), \quad (14)$$

$$\mathcal{L}_{\text{task}} = - \sum_{c=1}^C \hat{y}_c \log p_c, \mathcal{L}_{\text{rel}} = \sum_{t=1}^T \sum_{i=1}^N -y_{t,i} \log p_{\hat{\sigma}_{\text{rel}}(t,i)}. \quad (15)$$

Specifically, in the first stage, we train the Multi-Modal Scene Graph Decoder using the loss function \mathcal{L}_{rel} ; in the second stage, we apply the loss function $\mathcal{L}_{\text{task}}$ to perform end-to-end training of the entire model.

4. Experiments

4.1. Datasets and Evaluation Metrics.

Dataset. *MUSIC-AVQA* [27] contains 9,288 musical performance videos (22 instruments, ~ 150 hours) and 45,867 QA pairs, covering five question types (existential, counting, location, comparative, temporal) for audio-visual reasoning. *MUSIC-AVQA-v2.0* [34] extends this benchmark to 10,492 videos with separate training/validation/test splits and provides both biased and balanced subsets, enabling more reliable evaluation under diverse multi-instrument scenes.

Metrics. We use top-1 answer accuracy, counting a prediction as correct if it exactly matches the ground-truth answer. We report accuracy on *Audio QA*, *Visual QA*, and *Audio-Visual QA*, as well as the overall average. For finer-grained analysis, we additionally report per-category accuracy (*e.g.*, attribute, counting) as in the original benchmark.

4.2. Implementation Details

We implement our model based on PyTorch on a single NVIDIA RTX 3090 for 25 epochs with a batch size of 32. During the first 10 epochs, we train the Multi-Modal Scene Graph Decoder, then freeze it and train the remaining modules in the subsequent 15 epochs. The input videos are sampled at a rate of 1 fps. Audio features are extracted using VGGish [15], while visual features and questions are encoded with the CLIP-ViT/14 [47]. All features are linearly transformed to 512 dimensions to maintain consistency. In all experiments, we use the Adam optimizer with an initial

Method	Audio QA			Visual QA			Audio-Visual QA						Avg
	Count	Comp	Avg	Count	Local	Avg	Exist	Count	Local	Comp	Temp	Avg	
AVSD [48]	72.41	61.90	68.52	67.39	74.19	70.83	81.61	63.89	58.79	61.52	61.41	65.49	67.44
ST-AVQA [27]	78.18	67.05	74.06	71.56	76.38	74.00	81.81	70.80	64.51	66.01	63.23	69.54	71.52
COCA [25]	79.35	67.68	75.42	75.10	75.43	75.23	83.50	66.63	69.72	64.12	65.57	69.96	72.33
PSTP-Net [28]	73.97	65.59	70.91	77.15	77.36	77.26	76.18	72.23	71.80	71.79	69.00	72.57	73.52
LAVISH [32]	82.09	65.56	75.97	78.98	81.43	80.22	81.71	75.51	66.13	63.77	67.96	71.26	74.46
APL [31]	82.40	70.71	78.09	76.52	82.74	79.69	82.99	73.29	66.68	64.76	65.95	70.96	74.53
TSPM [29]	84.07	64.65	76.91	82.29	84.90	83.61	82.19	76.21	<u>71.85</u>	65.76	71.17	<u>73.51</u>	76.79
QA-TIGER†[24]	85.25	<u>68.01</u>	78.90	84.71	<u>86.29</u>	85.51	<u>82.49</u>	<u>78.74</u>	71.41	63.94	68.86	73.35	77.56
SHRIKE	85.84	<u>68.01</u>	79.27	85.30	86.86	86.09	80.26	79.05	72.72	<u>66.76</u>	<u>69.83</u>	74.00	78.14

Table 1. Comparison with state-of-the-art method on the MUSIC-AVQA [27] test set. The best-performing results are shown in **bold**, and the second-best results are underlined. † denotes results obtained by reproducing the model using official codes.

Test	Training	Method	A-QA	V-QA	AV-QA	Avg
Bias	Bias	LAVISH [32]	76.73	80.96	70.80	74.59
		QA-TIGER†[24]	78.94	84.99	72.63	77.08
		SHRIKE	78.39	86.09	72.73	77.33
	Balance	LAST-Att [34]	77.29	83.47	71.05	75.45
		QA-TIGER†[24]	78.39	85.93	71.68	76.71
		SHRIKE	78.82	87.40	71.30	76.97
Test	Training	Method	A-QA	V-QA	AV-QA	Avg
Balance	Bias	LAVISH [32]	73.14	79.70	65.01	70.39
		QA-TIGER†[24]	78.12	84.84	68.06	74.35
		SHRIKE	77.33	85.90	68.19	74.44
	Balance	LAST-Att [34]	78.56	84.07	70.30	75.44
		QA-TIGER†[24]	79.31	86.28	70.11	76.08
		SHRIKE	78.91	87.44	70.36	76.45

Table 2. Comparison with state-of-the-art methods on the Music-AVQA v2 dataset. The left table shows results on the biased test set, and the right table shows results on the balanced test set.

learning rate of $1e^{-4}$ and will drop by multiplying by 0.1 every 9 epochs. During scene graph extraction, the video is divided into 10 segments, and a scene graph is generated for each segment. In the proposed modules, we set $top_k = 10$. More details are provided in the supplementary materials.

4.3. Quantitative Results

We evaluate SHRIKE on MUSIC-AVQA and Music-AVQA v2.0, as shown in Table 1 and Table 2. **For MUSIC-AVQA [27]**, SHRIKE achieves state-of-the-art performance on the overall Avg (78.14%), excelling in most subsets. For example, in the Local task of the Audio-Visual QA subset, it surpasses QA-TIGER [24] by 1.31% (72.72% vs 71.41%). **For MUSIC-AVQA v2.0**, SHRIKE achieves state-of-the-art results across most subsets. In the overall Avg of all subsets, our method consistently leads (77.33% vs 77.08%, 76.98% vs 76.71%, 74.44% vs 74.35%, 76.45% vs 76.08%). These results highlight the strong reasoning capabilities of our method.

4.4. Ablation Studies

Multimodal Scene Graph and KAN-based MoE. We conduct ablation experiments on our two core compo-

Dataset	Method	A-QA	V-QA	AVQA	Average
MUSIC-AVQA (subset)	Ours w/ MiniCPM-o	70.55	74.94	67.22	69.83
MUSIC-AVQA (subset)	Ours w/ Qwen2.5 Omni	69.09	78.29	66.03	69.76
MUSIC-AVQA (full)	Only MiniCPM-o	50.96	58.06	37.71	40.00
MUSIC-AVQA (full)	Ours w/ MiniCPM-o	79.27	86.09	74.00	78.14

Table 4. Comparison using scene graph annotations generated by different MLLMs and direct QA performance of MiniCPM-o on the MUSIC-AVQA dataset.

nents— Temporal Integration with Gaussian KAN-based Experts and the Scene Graph Decoder—as shown in Table 3. After incorporating the Multi-Modal Scene Graph, the average accuracy improves by 1.13% (77.56% vs. 76.43%). When KAN is introduced into the Temporal Integration module, the average accuracy further increases by 0.58% (78.14% vs. 77.56%).

Selection of KAN Experts. We investigate the impact of the number of KAN experts on the experimental results, as shown in Figure 5. The model achieves its best performance when the quantity is set to 7. Furthermore, by comparing our method with QA-TIGER [24], our approach consistently outperforms QA-TIGER [24], demonstrating that KAN-based temporal integration is more effective than MLP-based temporal integration.

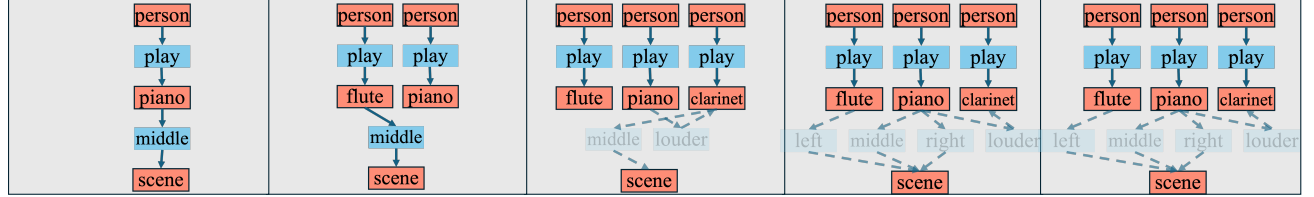
Selection of Relationship Triplets. We examine the impact of the number of relationship triplet sets selected per frame (top_k). The result is shown in Figure 6. When top_k is set to 8, the model achieves an accuracy of 77.69%, surpassing the state-of-the-art QA-Tiger model. When top_k is increased to 10, the accuracy improves to 78.14%, highlighting the advantages of the selection of the relationship triplet.

4.5. Analysis of Temporal Integration

In this section, we evaluate whether the model accurately identifies the time segments relevant to the question by visualizing the Gaussian distributions of the visual and auditory modalities. As illustrated in Figure 4a, and Figure 4b, we provide a qualitative analysis of its performance. The blue curves denote our KAN-based temporal integration module,



(a) What is the **first** instrument that comes in? **Ground Truth: Piano** **QA-TIGER: Violin** **Ours: Piano**



(b) Where is the **loudest** instrument? **Ground Truth: Left** **QA-TIGER: Middle** **Ours: Middle**

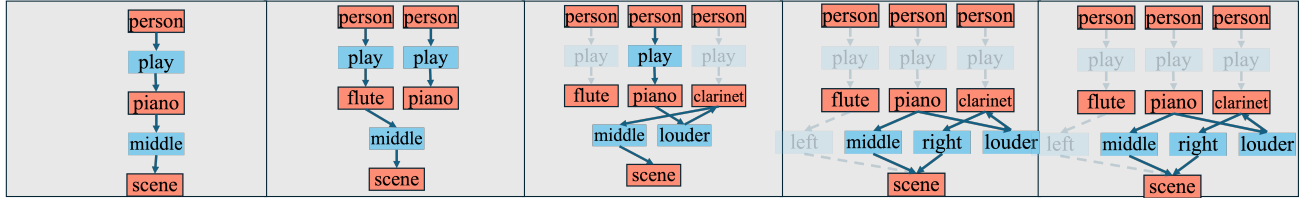


Figure 3. Visualized relationship triplet selection results. In the given example, we convert all the relationship triplets into a scene graph and highlight the triplets selected by our method.

M ² SG	KAN	A-QA	V-QA	AV-QA	Avg
✓		77.96	83.44	72.50	76.43
	✓	78.52	86.13	73.18	77.56
✓	✓	78.09	85.57	73.21	77.33
		79.27	86.09	74.00	78.14

Table 3. Ablation study of the proposed framework. M²SG is Multi-Modal Scene Graph Module.

while the red curves are those from QA-TIGER [24].

Visual Question. As shown in Figure 4a, both QA-TIGER [24] and SHRIKE successfully identified the appearance of the piano in region A through visual cues (both blue and red distributions exhibit high values). However, QA-TIGER [24] failed to detect the second instrument, cello, in region B in visual cues, leading to an incorrect result. While QA-TIGER [24] identifies one instrument in the visual stream and another in the audio stream, our proposed SHRIKE, by incorporating structured visual information, simultaneously detected both instruments across both modalities (regions A and B for visual, regions C and D for audio), ultimately yielding the correct answer.

Audio-Visual Question. As shown in Figure 4b, for a problem simultaneously related to audio and visual modalities, the model needs to integrate cues from both audio and visual modalities for reasoning. From the visual cues, although both QA-TIGER [24] and our method detected the appearance of the trumpet, our proposed approach, leveraging structured visual information, captured the cue earlier (region E vs region F), which is crucial for determin-

ing whether it is always playing. Simultaneously, from the audio cues, our method also identified the sound cue earlier (region G vs region H). The tighter complementarity between audio and visual information enabled our model to arrive at the correct answer, demonstrating its superior audio-visual modeling capabilities. Overall, the clearer and earlier peaks of the blue curves indicate that the KAN-based temporal integration learns more discriminative and better aligned temporal weights than the MLP-based counterpart, highlighting the stronger expressive power of KAN experts for modeling complex cross-modal temporal dependencies.

4.6. Qualitative Results.

Figure 3 illustrates the visualized predictions of QA-TIGER [24] and our SHRIKE, for the same audio-visual input, along with the generated multi-modal scene graphs. **In Figure 3 (a)**, given the question “What is the first instrument that comes in?”, our model accurately identified the first appearing instrument, piano, and retained all relevant prediction values, such as $\langle \text{person}, \text{play}, \text{piano} \rangle$ and $\langle \text{piano}, \text{louder than}, \text{flute} \rangle$. It enhances the model’s ability to structurally understand visual information. **In Figure 3 (b)**, for the question “Where is the loudest instrument?”, the model produced an incorrect answer. While it correctly retained triplets related to positional information and sound volume, the absence of comparative relations with other instruments during scene graph generation led to the erroneous preservation of triplets like $\langle \text{piano} - \text{louder than} - \text{clarinet} \rangle$ and $\langle \text{piano} - \text{left} - \text{scene} \rangle$, resulting in an incorrect inference. This error mainly stems

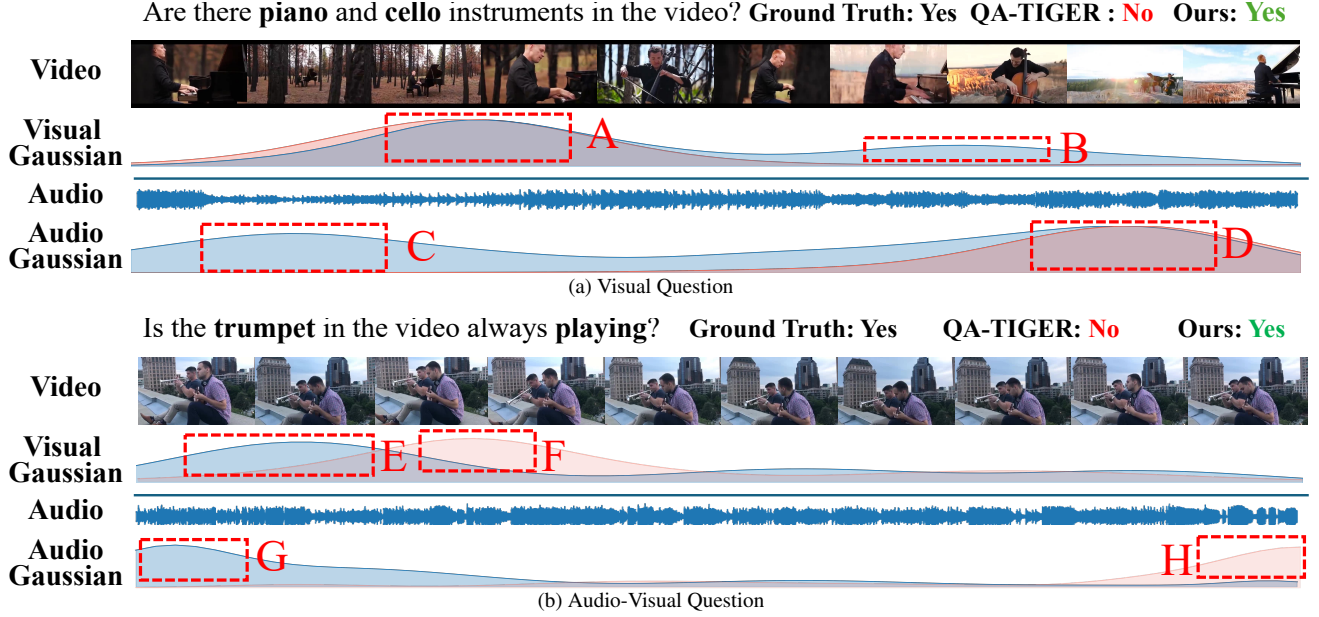


Figure 4. Comparison of key temporal segment capture between SHRIKE and QA-TIGER. Blue wavy lines represent SHRIKE and Red wavy lines represent QA-TIGER.

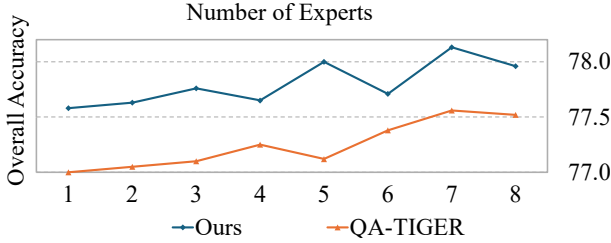


Figure 5. Model performance with numbers of KAN experts.

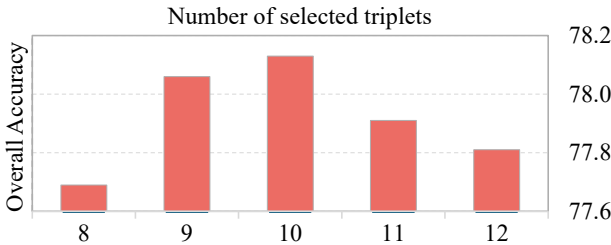


Figure 6. Model performance with different top_k values.

from the long-tail distribution of audio loudness. The model cannot reliably capture the relative volume of less salient instruments, causing some key audio triplets to be missed during scene graph generation and ultimately leading to an incorrect answer.

4.7. Discussion

Transfer into Audio-Visual Event Localization. To further assess the generalization ability of our model, we evaluate the proposed M²SG on the audio-visual event localization task using the Audio-Visual Event (AVE)

dataset [51]. Under the standard setting where both audio and visual modalities are available, our method achieves slightly higher performance than CACE-Net [14] (78.61% vs. 78.48%). These results indicate that M²SG not only performs well on our primary task, but also transfers effectively to downstream audio-visual event localization, demonstrating strong generalization capability across related audio-visual event understanding tasks.

Choice of MLLM for Multimodal Scene Graph Annotation. To choose an MLLM for automatic scene graph annotation, we compare MiniCPM-o and Qwen2.5 Omni [54] on the same 2,000 annotated videos under identical training and evaluation settings. As shown in Table 4, MiniCPM-o achieves slightly better overall performance and is much faster at inference (about 5 s vs. 30 s per video), so we adopt MiniCPM-o as the default MLLM in our experiments.

Performance of MiniCPM-o on the MUSIC-AVQA Dataset. To estimate how much task-specific supervision MiniCPM-o injects through pseudo scene graph annotations, we also evaluate it directly on the MUSIC-AVQA QA task. As shown in Table 4, MiniCPM-o achieves only about 40% accuracy, far below supervised audio-visual QA models. This suggests that its scene graph annotations provide coarse semantic cues rather than near-oracle labels, and do not leak substantial ground-truth information into our framework.

5. Conclusion

In this paper, we presented a framework that combines multi-modal scene graphs with KAN for audio-visual ques-

tion answering, where a Scene Graph Decoder to extract relation triplets from fused audio–visual features, and a KAN-based Mixture-of-Experts for modeling complex cross-modal temporal dependencies. Extensive experiments on both datasets demonstrate the effectiveness and superiority.

References

- [1] *Elements of the theory of functions and functional analysis*. Courier Corporation, 1957. 2
- [2] Huda Alamri, Vincent Cartillier, Abhishek Das, Jue Wang, Anoop Cherian, Irfan Essa, Dhruv Batra, Tim K Marks, Chiori Hori, Peter Anderson, et al. Audio visual scene-aware dialog. In *Proceedings of the IEEE/CVF Conference on Computer Vision and Pattern Recognition*, pages 7558–7567, 2019. 2
- [3] Daniel Bolya, Cheng-Yang Fu, Xiaoliang Dai, Peizhao Zhang, Christoph Feichtenhofer, and Judy Hoffman. Token merging: Your vit but faster. *arXiv preprint arXiv:2210.09461*, 2022. 4, 2
- [4] Nicolas Carion, Francisco Massa, Gabriel Synnaeve, Nicolas Usunier, Alexander Kirillov, and Sergey Zagoruyko. End-to-end object detection with transformers. In *European conference on computer vision*, pages 213–229. Springer, 2020. 5
- [5] Jiaqi Chen, Daniel Barath, Iro Armeni, Marc Pollefeys, and Hermann Blum. “where am i?” scene retrieval with language. In *European Conference on Computer Vision*, pages 201–220. Springer, 2024. 2
- [6] Zailong Chen, Lei Wang, Peng Wang, and Peng Gao. Question-aware global-local video understanding network for audio-visual question answering. *IEEE Transactions on Circuits and Systems for Video Technology*, 34(5):4109–4119, 2023. 1
- [7] Wei Deng, Mengshi Qi, and Huadong Ma. Global-local tree search in vlms for 3d indoor scene generation. In *Proceedings of the Computer Vision and Pattern Recognition Conference*, pages 8975–8984, 2025. 2
- [8] Nan Du, Yanping Huang, Andrew M Dai, Simon Tong, Dmitry Lepikhin, Yuanzhong Xu, Maxim Krikun, Yanqi Zhou, Adams Wei Yu, Orhan Firat, et al. Glam: Efficient scaling of language models with mixture-of-experts. In *International conference on machine learning*, pages 5547–5569. PMLR, 2022. 5
- [9] Haoyi Duan, Yan Xia, Zhou Mingze, Li Tang, Jieming Zhu, and Zhou Zhao. Cross-modal prompts: Adapting large pre-trained models for audio-visual downstream tasks. *Advances in Neural Information Processing Systems*, 36:56075–56094, 2023. 1
- [10] Magdalena Fuentes, Bea Steers, Pablo Zinemanas, Martin Rocamora, Luca Bondi, Julia Wilkins, Qianyi Shi, Yao Hou, Samarjit Das, Xavier Serra, et al. Urban sound & sight: Dataset and benchmark for audio-visual urban scene understanding. In *ICASSP 2022-2022 IEEE International Conference on Acoustics, Speech and Signal Processing (ICASSP)*, pages 141–145. IEEE, 2022. 1
- [11] Yury Furlotov, Volker Willert, and Jürgen Adamy. Auditory scene understanding for autonomous driving. In *2021 IEEE Intelligent Vehicles Symposium (IV)*, pages 697–702. IEEE, 2021. 1
- [12] Junyu Gao, Hao Yang, Maoguo Gong, and Xuelong Li. Audio–visual representation learning for anomaly events detection in crowds. *Neurocomputing*, 582:127489, 2024. 1
- [13] Ruohan Gao, Tae-Hyun Oh, Kristen Grauman, and Lorenzo Torresani. Listen to look: Action recognition by previewing audio. In *Proceedings of the IEEE/CVF conference on computer vision and pattern recognition*, pages 10457–10467, 2020. 2
- [14] Xiang He, Xiangxi Liu, Yang Li, Dongcheng Zhao, Guobin Shen, Qingqun Kong, Xin Yang, and Yi Zeng. Cace-net: Co-guidance attention and contrastive enhancement for effective audio-visual event localization. In *Proceedings of the 32nd ACM International Conference on Multimedia*, pages 985–993, 2024. 8
- [15] Shawn Hershey, Sourish Chaudhuri, Daniel PW Ellis, Jort F Gemmeke, Aren Jansen, R Channing Moore, Manoj Plakal, Devin Platt, Rif A Saurous, Bryan Seybold, et al. Cnn architectures for large-scale audio classification. In *2017 IEEE international conference on acoustics, speech and signal processing (icassp)*, pages 131–135. IEEE, 2017. 4, 5
- [16] Shengding Hu, Yuge Tu, Xu Han, Chaoqun He, Ganqu Cui, Xiang Long, Zhi Zheng, Yewei Fang, Yuxiang Huang, Weilin Zhao, et al. Minicpm: Unveiling the potential of small language models with scalable training strategies. *arXiv preprint arXiv:2404.06395*, 2024. 5
- [17] Chao Huang, Yapeng Tian, Anurag Kumar, and Chenliang Xu. Egocentric audio-visual object localization. In *Proceedings of the IEEE/CVF Conference on Computer Vision and Pattern Recognition*, pages 22910–22921, 2023. 2
- [18] Songtao Huang, Zhen Zhao, Can Li, and LEI BAI. TimeKAN: KAN-based frequency decomposition learning architecture for long-term time series forecasting. In *The Thirteenth International Conference on Learning Representations*, 2025. 2
- [19] Yuanyuan Jiang and Jianqin Yin. Clip-powered tass: Target-aware single-stream network for audio-visual question answering. *International Journal of Computer Vision*, 133(5): 2581–2598, 2025. 1
- [20] Justin Johnson, Ranjay Krishna, Michael Stark, Li-Jia Li, David Shamma, Michael Bernstein, and Li Fei-Fei. Image retrieval using scene graphs. In *Proceedings of the IEEE Conference on Computer Vision and Pattern Recognition (CVPR)*, 2015. 1
- [21] Justin Johnson, Ranjay Krishna, Michael Stark, Li-Jia Li, David Shamma, Michael Bernstein, and Li Fei-Fei. Image retrieval using scene graphs. In *Proceedings of the IEEE conference on computer vision and pattern recognition*, pages 3668–3678, 2015. 1, 2, 3
- [22] Justin Johnson, Bharath Hariharan, Laurens Van Der Maaten, Li Fei-Fei, C Lawrence Zitnick, and Ross Girshick. Clevr: A diagnostic dataset for compositional language and elementary visual reasoning. In *Proceedings of the IEEE conference on computer vision and pattern recognition*, pages 2901–2910, 2017. 2
- [23] Evangelos Kazakos, Arsha Nagrai, Andrew Zisserman, and Dima Damen. Epic-fusion: Audio-visual temporal bind-

- ing for egocentric action recognition. In *Proceedings of the IEEE/CVF international conference on computer vision*, pages 5492–5501, 2019. 2
- [24] Hongyeob Kim, Inyoung Jung, Dayoon Suh, Youjia Zhang, Sangmin Lee, and Sungeun Hong. Question-aware gaussian experts for audio-visual question answering. *arXiv preprint arXiv:2503.04459*, 2025. 2, 4, 5, 6, 7, 3
- [25] Mingrui Lao, Nan Pu, Yu Liu, Kai He, Erwin M Bakker, and Michael S Lew. Coca: Collaborative causal regularization for audio-visual question answering. In *Proceedings of the AAAI conference on artificial intelligence*, pages 12995–13003, 2023. 2, 6
- [26] Dmitry Lepikhin, HyoukJoong Lee, Yuanzhong Xu, Dehao Chen, Orhan Firat, Yanping Huang, Maxim Krikun, Noam Shazeer, and Zhifeng Chen. Gshard: Scaling giant models with conditional computation and automatic sharding. *arXiv preprint arXiv:2006.16668*, 2020. 5
- [27] Guangyao Li, Yake Wei, Yapeng Tian, Chenliang Xu, Ji-Rong Wen, and Di Hu. Learning to answer questions in dynamic audio-visual scenarios. In *Proceedings of the IEEE/CVF Conference on Computer Vision and Pattern Recognition*, pages 19108–19118, 2022. 1, 5, 6
- [28] Guangyao Li, Wenxuan Hou, and Di Hu. Progressive spatio-temporal perception for audio-visual question answering. In *Proceedings of the 31st ACM international conference on multimedia*, pages 7808–7816, 2023. 6, 3
- [29] Guangyao Li, Henghui Du, and Di Hu. Boosting audio visual question answering via key semantic-aware cues. In *Proceedings of the 32nd ACM International Conference on Multimedia*, pages 5997–6005, 2024. 6, 2, 3
- [30] Xiangyang Li and Shuqiang Jiang. Know more say less: Image captioning based on scene graphs. *IEEE Transactions on Multimedia*, 21(8):2117–2130, 2019. 2
- [31] Zhangbin Li, Dan Guo, Jinxing Zhou, Jing Zhang, and Meng Wang. Object-aware adaptive-positivity learning for audio-visual question answering. In *Proceedings of the AAAI Conference on Artificial Intelligence*, pages 3306–3314, 2024. 6
- [32] Yan-Bo Lin, Yi-Lin Sung, Jie Lei, Mohit Bansal, and Gedas Bertasius. Vision transformers are parameter-efficient audio-visual learners. In *Proceedings of the IEEE/CVF Conference on Computer Vision and Pattern Recognition*, pages 2299–2309, 2023. 1, 2, 6
- [33] Hongcheng Liu, Pingjie Wang, Yu Wang, and Yanfeng Wang. M2k-vdg: Model-adaptive multimodal knowledge anchor enhanced video-grounded dialogue generation. *arXiv preprint arXiv:2402.11875*, 2024. 2
- [34] Xiulong Liu, Zhikang Dong, and Peng Zhang. Tackling data bias in music-avqa: Crafting a balanced dataset for unbiased question-answering. In *Proceedings of the IEEE/CVF Winter Conference on Applications of Computer Vision*, pages 4478–4487, 2024. 5, 6
- [35] Ziming Liu, Yixuan Wang, Sachin Vaidya, Fabian Ruehle, James Halverson, Marin Soljačić, Thomas Y Hou, and Max Tegmark. Kan: Kolmogorov-arnold networks. 2025. 2
- [36] Changsheng Lv, Mengshi Qi, Liang Liu, and Huadong Ma. T2sg: Traffic topology scene graph for topology reasoning in autonomous driving. In *Proceedings of the Computer Vision and Pattern Recognition Conference*, pages 17197–17206, 2025. 1
- [37] Jie Ma, Min Hu, Pinghui Wang, Wangchun Sun, Lingyun Song, Hongbin Pei, Jun Liu, and Youtian Du. Look, listen, and answer: Overcoming biases for audio-visual question answering. *Advances in Neural Information Processing Systems*, 37:9507–9531, 2024. 1
- [38] Evonne Ng, Javier Romero, Timur Bagautdinov, Shaojie Bai, Trevor Darrell, Angjoo Kanazawa, and Alexander Richard. From audio to photoreal embodiment: Synthesizing humans in conversations. In *Proceedings of the IEEE/CVF Conference on Computer Vision and Pattern Recognition*, pages 1001–1010, 2024. 1
- [39] Mengshi Qi, Weijian Li, Zhengyuan Yang, Yunhong Wang, and Jiebo Luo. Attentive relational networks for mapping images to scene graphs. In *Proceedings of the IEEE/CVF Conference on Computer Vision and Pattern Recognition*, pages 3957–3966, 2019. 2
- [40] Mengshi Qi, Yunhong Wang, Annan Li, and Jiebo Luo. Stegan: Spatio-temporally coupled generative adversarial networks for predictive scene parsing. *IEEE Transactions on Image Processing*, 29:5420–5430, 2020. 2
- [41] Mengshi Qi, Jie Qin, Yi Yang, Yunhong Wang, and Jiebo Luo. Semantics-aware spatial-temporal binaries for cross-modal video retrieval. *IEEE Transactions on Image Processing*, 30:2989–3004, 2021. 1
- [42] Mengshi Qi, Changsheng Lv, and Huadong Ma. Robust disentangled counterfactual learning for physical audiovisual commonsense reasoning. *arXiv preprint arXiv:2502.12425*, 2025. 2
- [43] Mengshi Qi, Hao Ye, Jiaxuan Peng, and Huadong Ma. Action quality assessment via hierarchical pose-guided multi-stage contrastive regression. *arXiv preprint arXiv:2501.03674*, 2025. 1
- [44] Tianwen Qian, Jingjing Chen, Shaoxiang Chen, Bo Wu, and Yu-Gang Jiang. Scene graph refinement network for visual question answering. *IEEE Transactions on Multimedia*, 25:3950–3961, 2022. 2
- [45] Ruichen Qiu, Yibo Miao, Shiwen Wang, Yifan Zhu, Lijia Yu, and Xiao-Shan Gao. Powermlp: An efficient version of kan. In *Proceedings of the AAAI Conference on Artificial Intelligence*, pages 20069–20076, 2025. 2
- [46] Alec Radford, Jong Wook Kim, Chris Hallacy, Aditya Ramesh, Gabriel Goh, Sandhini Agarwal, Girish Sastry, Amanda Askell, Pamela Mishkin, Jack Clark, et al. Learning transferable visual models from natural language supervision. In *International conference on machine learning*, pages 8748–8763. PmLR, 2021. 4
- [47] Alec Radford, Jong Wook Kim, Chris Hallacy, Aditya Ramesh, Gabriel Goh, Sandhini Agarwal, Girish Sastry, Amanda Askell, Pamela Mishkin, Jack Clark, et al. Learning transferable visual models from natural language supervision. In *International conference on machine learning*, pages 8748–8763. PmLR, 2021. 5
- [48] Idan Schwartz, Alexander G Schwing, and Tamir Hazan. A simple baseline for audio-visual scene-aware dialog. In *Proceedings of the IEEE/CVF Conference on Computer Vision and Pattern Recognition*, pages 12548–12558, 2019. 6

- [49] Noam Shazeer, Azalia Mirhoseini, Krzysztof Maziarczyk, Andy Davis, Quoc Le, Geoffrey Hinton, and Jeff Dean. Outrageously large neural networks: The sparsely-gated mixture-of-experts layer. *arXiv preprint arXiv:1701.06538*, 2017. 2, 5
- [50] Jiaxin Shi, Hanwang Zhang, and Juanzi Li. Explainable and explicit visual reasoning over scene graphs. In *Proceedings of the IEEE/CVF conference on computer vision and pattern recognition*, pages 8376–8384, 2019. 2
- [51] Yapeng Tian, Jing Shi, Bochen Li, Zhiyao Duan, and Chenliang Xu. Audio-visual event localization in unconstrained videos. In *Proceedings of the European conference on computer vision (ECCV)*, pages 247–263, 2018. 8
- [52] Aisha Urooj, Hilde Kuehne, Bo Wu, Kim Chheu, Walid Bousselham, Chuang Gan, Niels Lobo, and Mubarak Shah. Learning situation hyper-graphs for video question answering. In *Proceedings of the IEEE/CVF Conference on Computer Vision and Pattern Recognition*, pages 14879–14889, 2023. 4
- [53] Kai Wang, Yapeng Tian, and Dimitrios Hatzinakos. Towards efficient audio-visual learners via empowering pre-trained vision transformers with cross-modal adaptation. In *Proceedings of the IEEE/CVF Conference on Computer Vision and Pattern Recognition*, pages 1837–1846, 2024. 1
- [54] Jin Xu, Zhifang Guo, Jinzheng He, Hangrui Hu, Ting He, Shuai Bai, Keqin Chen, Jialin Wang, Yang Fan, Kai Dang, et al. Qwen2. 5-omni technical report. *arXiv preprint arXiv:2503.20215*, 2025. 8
- [55] Zeyuan Yang, Jiageng Liu, Peihao Chen, Anoop Cherian, Tim K Marks, Jonathan Le Roux, and Chuang Gan. Rila: Reflective and imaginative language agent for zero-shot semantic audio-visual navigation. In *Proceedings of the IEEE/CVF Conference on Computer Vision and Pattern Recognition*, pages 16251–16261, 2024. 1
- [56] Yuan Yao, Tianyu Yu, Ao Zhang, Chongyi Wang, Junbo Cui, Hongji Zhu, Tianchi Cai, Haoyu Li, Weilin Zhao, Zhihui He, et al. Minicpm-v: A gpt-4v level mllm on your phone. *arXiv preprint arXiv:2408.01800*, 2024. 3, 1
- [57] Hao Ye, Mengshi Qi, Zhaohong Liu, Liang Liu, and Huadong Ma. Safedriverag: Towards safe autonomous driving with knowledge graph-based retrieval-augmented generation. In *Proceedings of the 33rd ACM International Conference on Multimedia*, pages 11170–11178, 2025. 1
- [58] Sangwoong Yoon, Woo Young Kang, Sungwook Jeon, SeongEun Lee, Changjin Han, Jonghun Park, and Eun-Sol Kim. Image-to-image retrieval by learning similarity between scene graphs. In *Proceedings of the AAAI Conference on Artificial Intelligence*, pages 10718–10726, 2021. 2
- [59] Jinxing Zhou, Jianyuan Wang, Jiayi Zhang, Weixuan Sun, Jing Zhang, Stan Birchfield, Dan Guo, Lingpeng Kong, Meng Wang, and Yiran Zhong. Audio-visual segmentation. In *European Conference on Computer Vision*, pages 386–403. Springer, 2022. 2
- [60] Pengfei Zhu, Mengshi Qi, Xia Li, Weijian Li, and Huadong Ma. Unsupervised self-driving attention prediction via uncertainty mining and knowledge embedding. In *Proceedings of the IEEE/CVF International Conference on Computer Vision*, pages 8558–8568, 2023. 1

Multi-Modal Scene Graph with Kolmogorov–Arnold Experts for Audio-Visual Question Answering

Supplementary Material

This Supplementary Material includes three components: the details of we proposed Multi-Modal Scene Graph Dataset in section 6, additional implementation details in section 7, and further visualization results in section 8.

6. Details of Multi-Modal Scene Graph Dataset

In this section, we present the configuration of object and predicate categories in the multi-modal scene graph dataset (section 6.1), along with the details of using MLLM for multi-modal scene graph generation (section 6.2).

6.1. Object and Predicate Categories Setting

We define 24 object categories in our Multi-Modal Scene Graph Dataset, consisting of the 22 most frequent musical instruments from the Music-AVQA dataset [27]—*cello*, *congas*, *pipa*, *ukulele*, *piano*, *accordion*, *clarinet*, *guzheng*, *saxophone*, *drum*, *violin*, *bagpipe*, *bassoon*, *acoustic_guitar*, *banjo*, *electric_bass*, *flute*, *trumpet*, *erhu*, *xylophone*, *tuba*, and *suona*—along with two general entities: *person* and *scene*, as shown in Table 5. These objects serve as nodes in our multi-modal scene graph.

Object Categories			
cello	congas	pipa	ukulele
piano	accordion	clarinet	guzheng
saxophone	drum	violin	bagpipe
bassoon	acoustic_guitar	banjo	electric_bass
flute	trumpet	erhu	xylophone
tuba	suona	person	scene

Table 5. Object categories in multi-modal scene graph dataset.

To capture rich semantic interactions in the Music-AVQA dataset [27], we define 6 predicate categories that primarily describe spatial configurations shown in Table 6, performer-instrument interactions, and auditory attributes. Unlike conventional scene graphs [20], our proposed multi-modal scene graphs jointly encode both visual and audio information.

Specifically, the spatial relations *left* and *right* represent the relative positions of musical instruments within video frames. The action relations *play* and *hold* require cross-modal reasoning: determining whether a person is playing an instrument involves analyzing visual cues (e.g., hand positions, posture) as well as audio evidence of the instrument being sounded. In contrast, *hold* indicates that a person

is holding an instrument without actively producing sound. Lastly, the auditory relation *louder* captures relative sound intensity between instruments. These predicate categories serve as edges in our multi-modal scene graph, forming $\langle \text{subject-predicate-object} \rangle$ triplets to represent relationships between objects. The distribution of these triplets is shown in Figure 7.

Spatial Relations	Action Relations	Auditory Relations
left right middle	play hold	louder

Table 6. Defined predicate categories in multi-modal scene graph dataset.

6.2. Multi-Modal Scene Graph Generation

MiniCPM-o. MiniCPM-o [56] is an efficient on-device multi-modal large language model (MLLM) with only 8B parameters. It supports real-time streaming processing of text, image, audio, and video modalities. The latest version, MiniCPM-o 2.6 [56], adopts a fully end-to-end multi-modal architecture that unifies the encoders and decoders of various modalities—text, image, audio, and video—into a single integrated framework. This unified design eliminates the complexity of traditional stage-wise multi-modal processing pipelines, enabling joint learning and efficient handling of multi-modal information.

Video Processing. After defining the object and predicate categories for the multi-modal scene graph, we employ MiniCPM-o 2.6 [56] to extract objects and predicates from the input videos. Specifically, we sample 10 one-second audiovisual clips from each video at six-second intervals, with the audio sampled at 16 kHz.

Scene Graph Generation. We focus on deriving relational triplets that capture key information and interactions among objects within the audiovisual scene. To this end, we first design tailored prompts that guide the model in identifying relevant triplet components. The model is prompted to recognize all objects present in each audiovisual clip, with numerically indexed instances used to distinguish multiple objects of the same category. The prompt as shown in Figure 8

For spatial relations, we constrain the vocabulary to terms such as *left*, *right*, and *middle*, which are used to describe the relative positioning of musical instruments in the

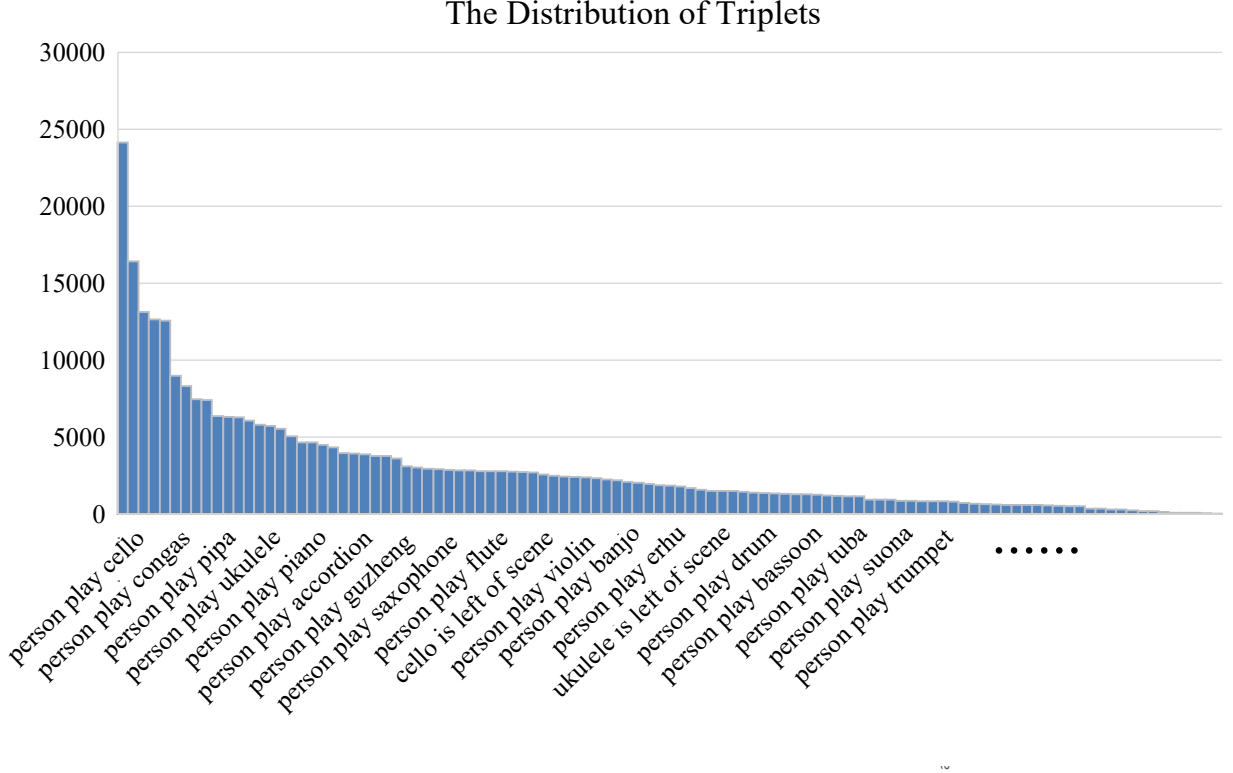


Figure 7. The Distribution of Triplets in the training set.

visual scene. The model is guided to determine these spatial relations based on visual inputs. To extract *play* and *hold* relations, we prompt the model to assess whether each instrument is actively played by a person, requiring joint reasoning over both visual content and auditory signals. For the *louder* relation, we instruct the model to compare the sound intensities of different instruments co-occurring in the same clip.

7. Additional Implementation Details

In this section, we present additional implementation details, including the patch merging method for visual tokens (Section 7.1), specific aspects of the model’s training strategy (Section 7.2), Runtime and Parameter Efficiency of SHRIKE (Section 7.3) and implementation details of the KAN experts (Section 7.4).

7.1. Patch Merge

We adopt the patch merging approach introduced in ToMe [3], where visually similar tokens are progressively combined at each transformer layer. This process partitions tokens into groups, computes pairwise similarities, and then applies an averaging mechanism to produce fused token representations. Incorporating this strategy ensures that our

feature extraction is consistent with baseline (TSPM [29]), maintaining alignment across the experimental design.

7.2. Training Strategy

In our model design, we argue that the prediction of scene graphs by the Multi-Modal Scene Graph Decoder (MMSG) should remain independent of the specific question being asked. To this end, we adopt a two-stage training strategy. In the first stage, we pre-train the MMSG module separately. Specifically, the input to the module consists of visual and audio features, while the output is a set of classification probabilities over triplets representing the scene graph for each video frame.

To optimize the model, we employ the Hungarian loss, which effectively handles permutation-invariant triplet matching. During training, we assume a fixed number of 12 triplets per clip. If the number of valid triplets is fewer than 12, we pad the missing entries with a special *None* token. Through this procedure, we obtain a robust MMSG module capable of accurately predicting multi-modal scene graph structures without being influenced by question-specific information. To prevent the model from overfitting to padded entries, we assign a lower loss weight of 0.3 to *None* triplets, while valid triplets are assigned a weight of 1. The model is trained for 15 epochs using the Adam optimizer with an

Prompt for Multi-Modal Scene Graph Generation

Given a video which has 10 clips and a list of relationships, identify all instruments from the video, their attributes and all relationships among these entities.

Audio-Relationships: [person play cello, person hold cello, person play congas, person hold congas, person play pipa, person hold pipa, ... cello is louder than congas, flute is louder than piano ... (All audio-relationship can be found in Audio-Relationships.txt)]

Visual-Relationships: [cello is left of scene, cello is right of scene, cello is medium of scene, congas is left of scene, congas is right of scene, ..., (All visual-relationship can be found in Visual-Relationships.txt)]

For each clip:

Step 1. Format follows:

- clip_id: the sequence of clips(e.g., <clip_1>)

Step 2. Identify instruments:

Accurately identify the type of all musical instruments and players in the clip.

Step 3. Identify Relationships:

Select the combinations from the list that match the current situation. Format Relationships as <Relationships>

- Audio-triplets: Select from the Audio-Relationships. Each clip has no less than 4 Audio-triplets. The relationships must match the current clip's situation. Audio-triplets as <Audio-Relationship>

- Visual-triplets: Select from the Visual-Relationships. Each clip has no less than 4 Visual-triplets. The relationships must match the current clip's situation. Format Visual-triplets as <Visual-Relationships>

Step 3. Format each clip

After relationships are identified, format each clips as **(<clips id>:<Audio-Relationship> <Visual-Relationships> **. (e.g., <clip_1>:person play cello, person play tuba, cello is louder than tuba, cello is left of scene, tuba is right of scene)

Step 4. output

Return output in English as a list of 10 clips.

Figure 8. Prompt to MiniCPM-o 2.6 [56] for Multi-Modal Scene Graph Generation.

initial learning rate of $1e^{-4}$, which is decayed by a factor of 0.1 every 5 epochs.

In the second stage, we freeze the parameters of the pre-trained MMSG module and train the remaining components of the model. At this stage, the model takes visual and audio features, along with the question embedding, as input, and predicts the answer by outputting classification probabilities over candidate answers. We use the cross-entropy loss to supervise the training. The model is trained for 15 epochs using the Adam optimizer with an initial learning rate of $1e^{-4}$, which is decayed by a factor of 0.1 every 9 epochs to stabilize training and facilitate convergence.

We also evaluated all models under different encoder backbones. As shown in Fig 7, our method consistently achieves the best performance across all encoder configurations

Method	CLIP Encoder	A-QA	V-QA	AV-QA	Avg
PSTP-Net[28]	B/32	70.91	77.26	72.57	73.52
TSPM[29]	B/32	76.91	81.92	72.57	75.81
QA-TIGER[24]	B/32	76.23	84.10	72.14	76.03
Ours	B/32	78.15	83.86	72.23	76.36

Table 7. Performance with different encoders serving both visual and text feature extraction.

7.3. Runtime and Parameter Efficiency

On the Music-AVQA dataset, our SHRIKE model requires about 3 minutes per epoch during the first training stage (10 epochs total), and about 6 minutes per epoch during the second stage (15 epochs total), resulting in a total training time of roughly 2 hours. For inference, SHRIKE takes around 33 seconds on an NVIDIA RTX 3090 GPU (batch size 32).

Algorithm 1 Gaussian KAN Experts Module

Input: Question features: $q_s \in \mathbb{R}^D$. Video features: $v_q \in \mathbb{R}^{T \times D}$. Audio features: $a_q \in \mathbb{R}^{T \times D}$. Patch features: $p_v, p_a \in \mathbb{R}^{T \times D}$.

Output: Temporal integrated features: Aggregated visual-related patch features $\widetilde{F}_{p_v} \in \mathbb{R}^D$, aggregated audio-related patch features $\widetilde{F}_{p_a} \in \mathbb{R}^D$. Aggregated audio features $\widetilde{F}_a \in \mathbb{R}^D$.

Initialization: Initialize the center of E experts to the central positions of E segments.

$$\text{margin} = \frac{1}{2E}$$

for $i = 0$ **to** $E - 1$ **do**

$$\mu_{\text{fixed}}[i] = \text{margin} + i \cdot \frac{1 - 2 \cdot \text{margin}}{E - 1}$$

end for

Question-driven Attention:

$$v'_q = \text{CA}(q_s, v_q, v_q), a'_q = \text{CA}(q_s, a_q, a_q)$$

Experts Router:

$$r_v = \text{Softmax}(\text{Linear}(\mathbf{v}'_q)),$$

$$r_a = \text{Softmax}(\text{Linear}(\mathbf{a}'_q))$$

Gaussian Weight Generation:

$$\mu_{\text{offset}|v}, \sigma_v = \text{FC}(v'_q), \mu_{\text{offset}|a}, \sigma_a = \text{FC}(a'_q)$$

Adjust centers and normalize widths:

for $i = 0$ **to** $E - 1$ **do**

$$\mu_v[i] = \mu_{\text{fixed}}[i] + \text{Tanh}(\mu_{\text{offset}|v}[i]) \cdot \text{margin}$$

$$\mu_a[i] = \mu_{\text{fixed}}[i] + \text{Tanh}(\mu_{\text{offset}|a}[i]) \cdot \text{margin}$$

$$\sigma_v[i] = \text{sigmoid}(\sigma_v[i]),$$

$$\sigma_a[i] = \text{sigmoid}(\sigma_a[i])$$

end for

Generate temporal Gaussian weights:

for $i = 0$ **to** $E - 1$ **do**

$$g_v[i] = \mathcal{N}(\mu_v[i], \sigma_v[i]^2),$$

$$g_a[i] = \mathcal{N}(\mu_a[i], \sigma_a[i]^2),$$

$$g_v[i] = \frac{g_v[i]}{\max(g_v[i])}, g_a[i] = \frac{g_a[i]}{\max(g_a[i])}$$

end for

Integration of KAN Experts Output:

$$p_v = \mathbf{v}_q + p_v$$

$$p_a = \mathbf{v}_q + p_a$$

$$\widetilde{F}_a = \sum_{i=0}^{E-1} g_a[i] \cdot r_a[i] \cdot \mathcal{F}_{\text{KAN}}^i(a_q)$$

$$\widetilde{F}_{p_v} = \sum_{i=0}^{E-1} g_v[i] \cdot r_v[i] \cdot \mathcal{F}_{\text{KAN}}^i(p_v)$$

$$\widetilde{F}_{p_a} = \sum_{i=0}^{E-1} g_v[i] \cdot r_v[i] \cdot \mathcal{F}_{\text{KAN}}^i(p_a)$$

return $\widetilde{F}_a, \widetilde{F}_{p_v}, \widetilde{F}_{p_a}$

7.4. Details of the KAN Experts

Inspired by QA-TIGER [24], we initialize the Gaussian centers of experts μ_{fixed} as E points spaced at fixed intervals as shown in algorithm 1. By applying learnable offsets

to the fixed positions, the centers are adjusted within restricted margins. This guarantees that each expert attends to unique temporal intervals, improving the effectiveness of capturing relevant segments and minimizing redundancy, thereby maintaining the specialization of each expert.

8. Further Visualization Results

As shown in Figure 9 and Figure 10, we present more visualization results comparing our proposed method with other baseline models. It can be seen from the figures that our proposed method outperforms the original method.

In Figure 9a, SHRIKE’s visual Gaussian attention correctly focuses on the frame where three violins appear simultaneously in Region B, whereas QA-TIGER misplaces its attention on an incorrect frame in Region A. In addition to visual attention, SHRIKE’s audio Gaussian mechanism accurately focuses on the segment where three violins are playing at the same time, highlighting its superior multi-modal reasoning ability in Region C. In Figure 9b, SHRIKE’s audio Gaussian attention broadly attends to all audio frames, which aligns with the fact that the piano and violin are playing simultaneously throughout the entire clip in Region E and Region F. For Figure 9c, SHRIKE demonstrates a more accurate visual understanding by first identifying the frame in which three acoustic guitars are present simultaneously. QA-TIGER, on the other hand, mistakenly attends to a frame where only a person is present in the scene graph, which ultimately results in an incorrect prediction.

In Figure 10, SHRIKE answers the question by assessing whether the flute is being played at each moment. The model accurately predicts that in the middle clip of the video, the person is not playing the flute. As shown in the figure 10(a), it predicts the relation $\textit{person-hold-flute}$ instead of $\textit{person-play-flute}$. On the other hand, the model accurately predicts both $\textit{person-play-flute}$ and $\textit{person-play-cello}$ in the video frames, which directly supports answering the question: “Which musical instrument sounds at the same time as the flute?” as show in Figure 10(b). We also present more visualization results in Figure 11, Figure 12, Figure 13 and Figure 14.

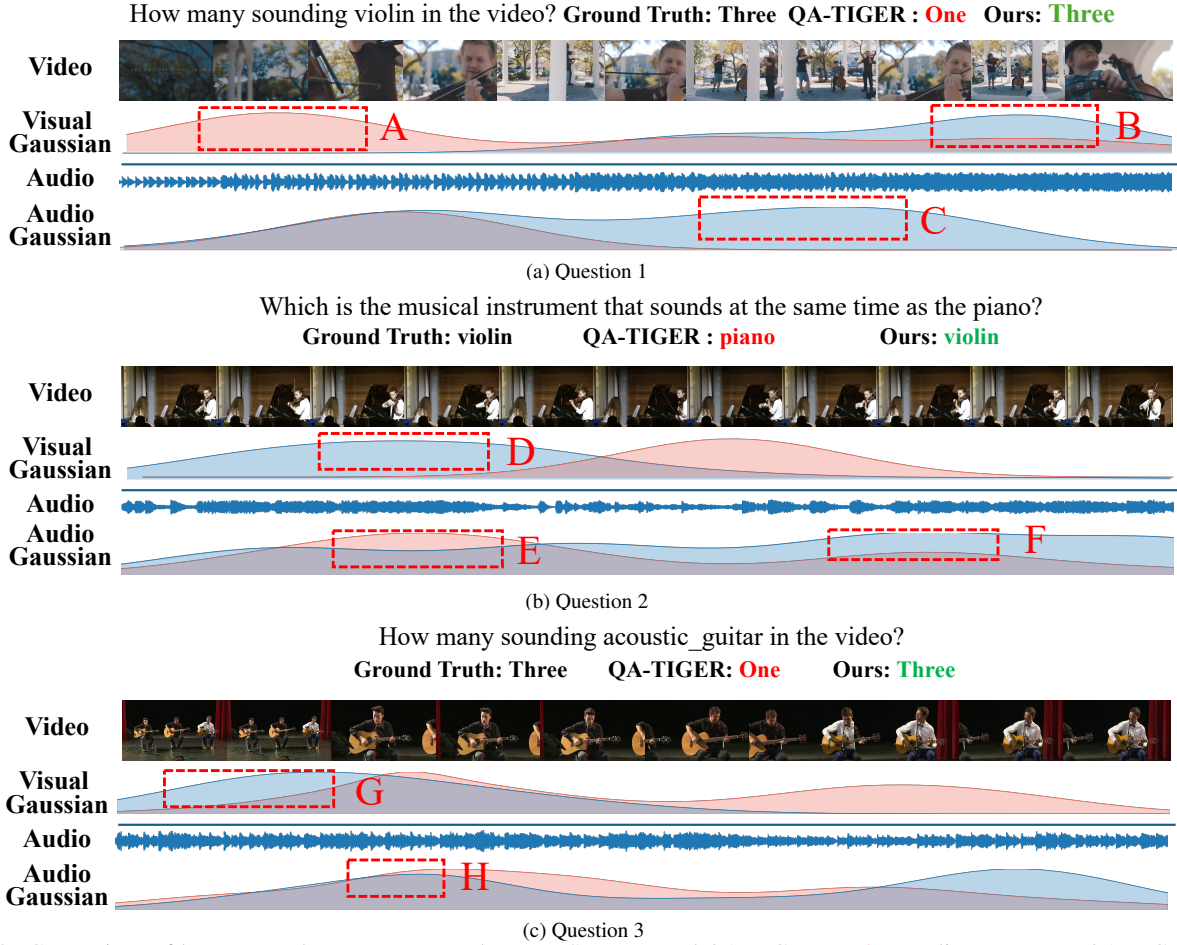


Figure 9. Comparison of key temporal segment capture between SHRINK and QA-TIGER. Red wavy lines represent QA-TIGER, and blue wavy lines represent SHRINK.

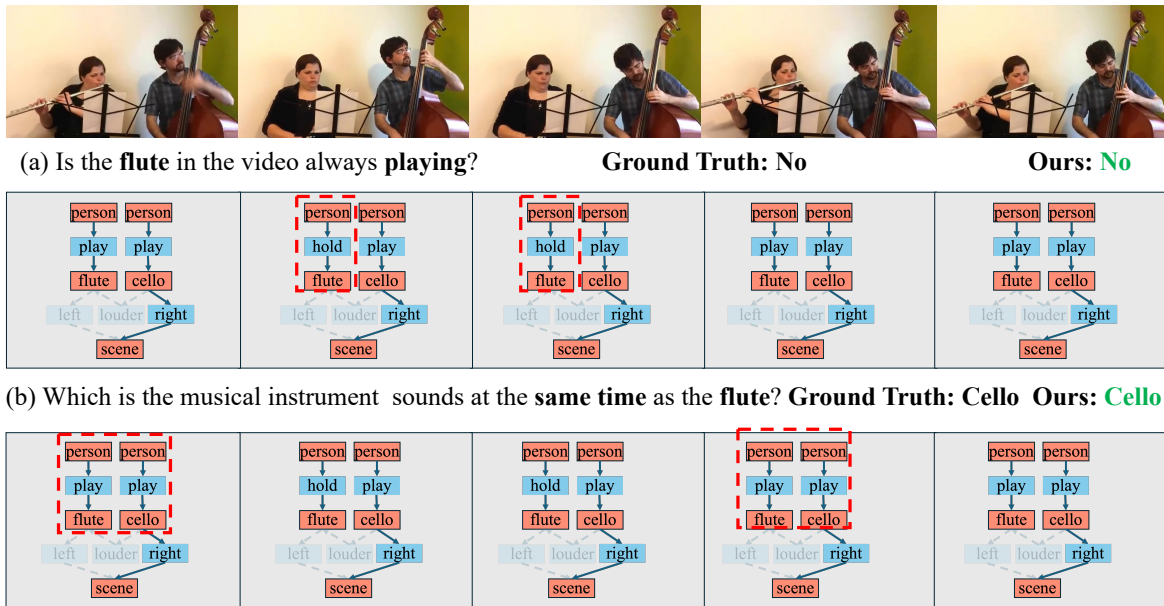


Figure 10. Visualized relationship triplet selection result. In the given example, we convert all the relationship triplets into a scene graph and highlight the triplets selected by our method.

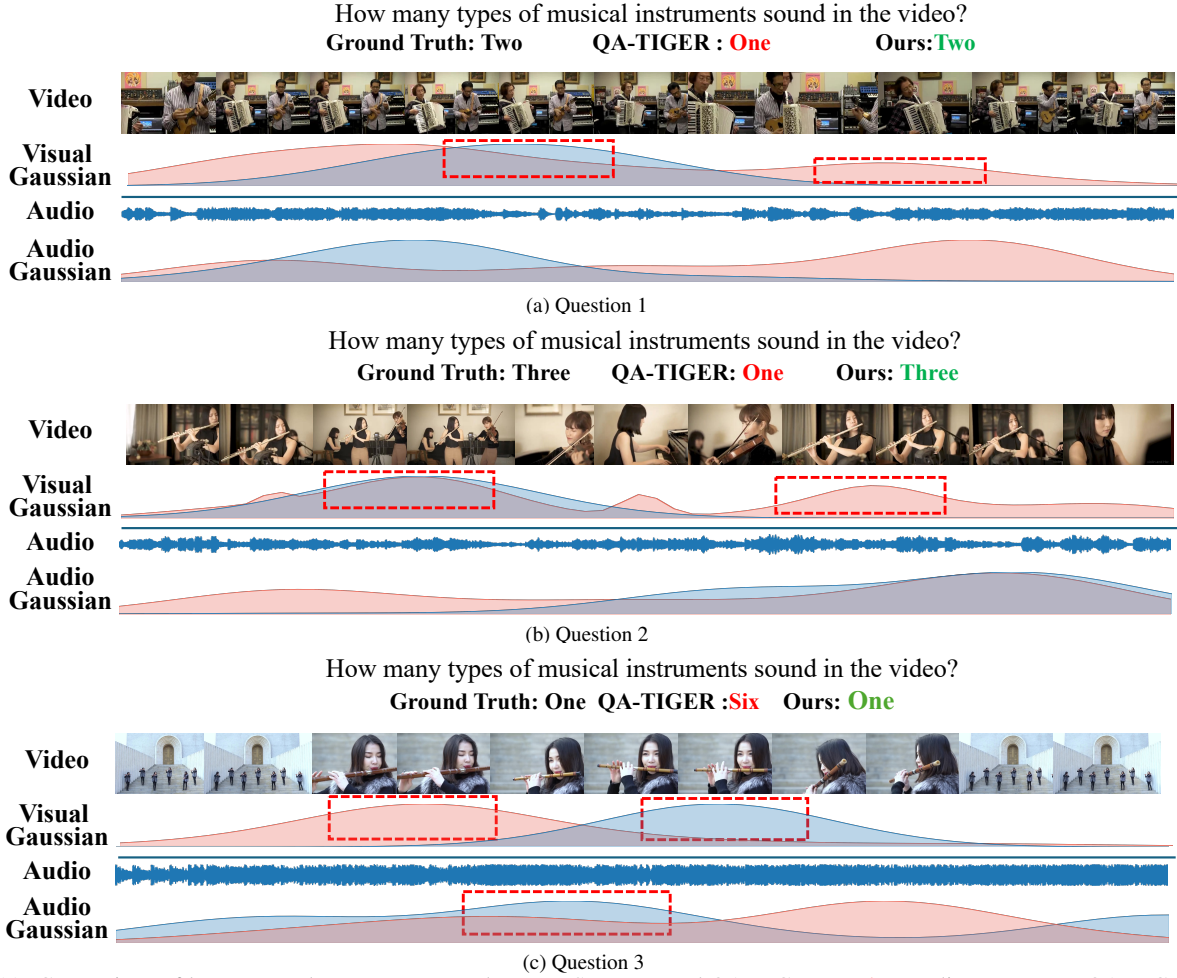


Figure 11. Comparison of key temporal segment capture between SHRINK and QA-TIGER. Red wavy lines represent QA-TIGER, and blue wavy lines represent SHRINK.

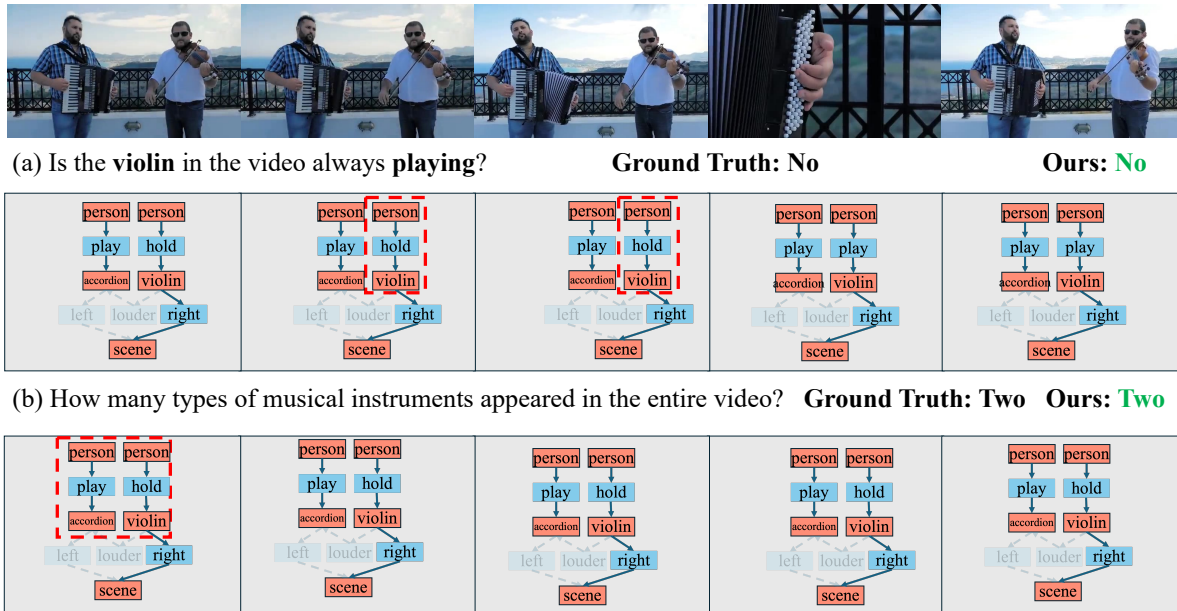


Figure 12. Visualized relationship triplet selection result. In the given example, we convert all the relationship triplets into a scene graph and highlight the triplets selected by our method.

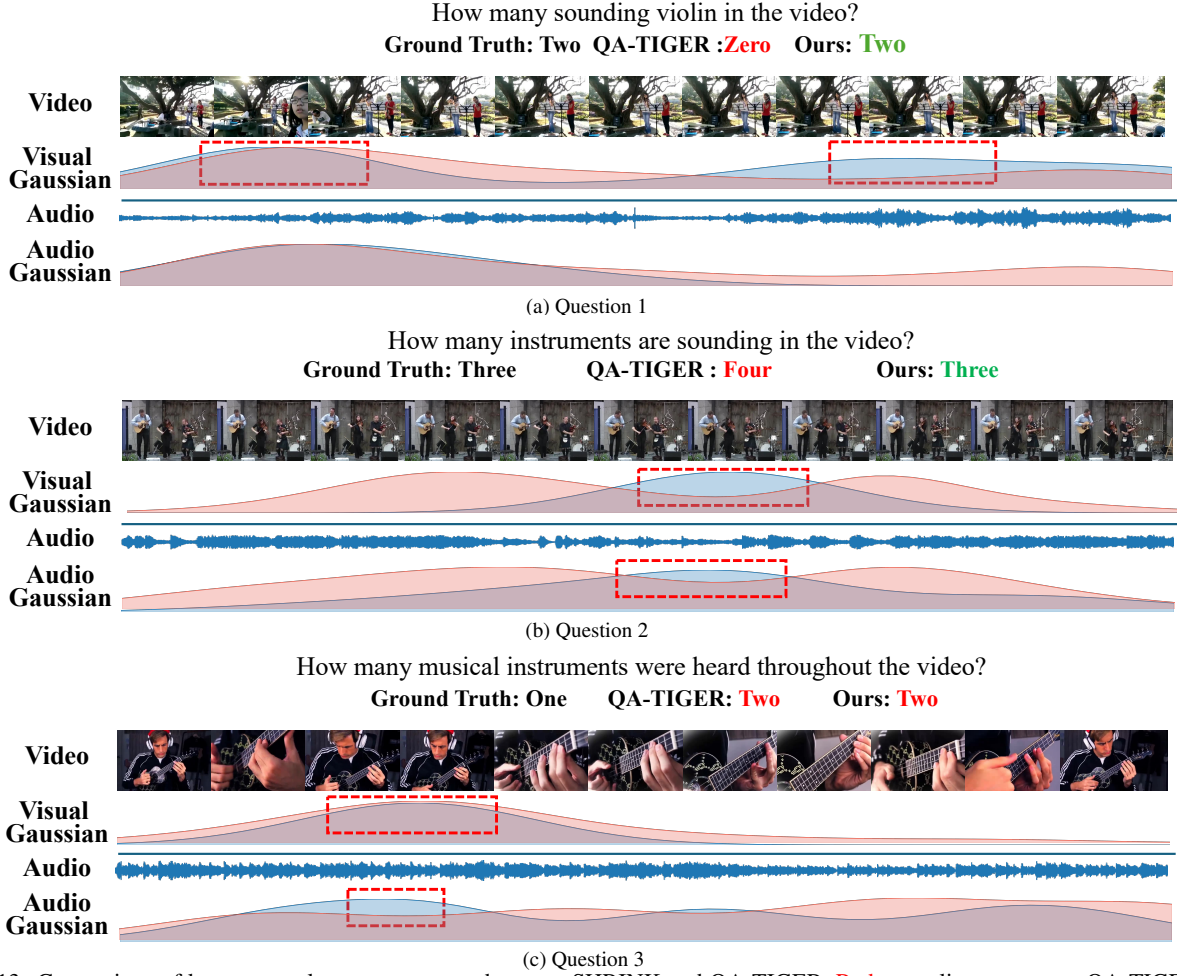


Figure 13. Comparison of key temporal segment capture between SHRINK and QA-TIGER. Red wavy lines represent QA-TIGER, and blue wavy lines represent SHRINK.

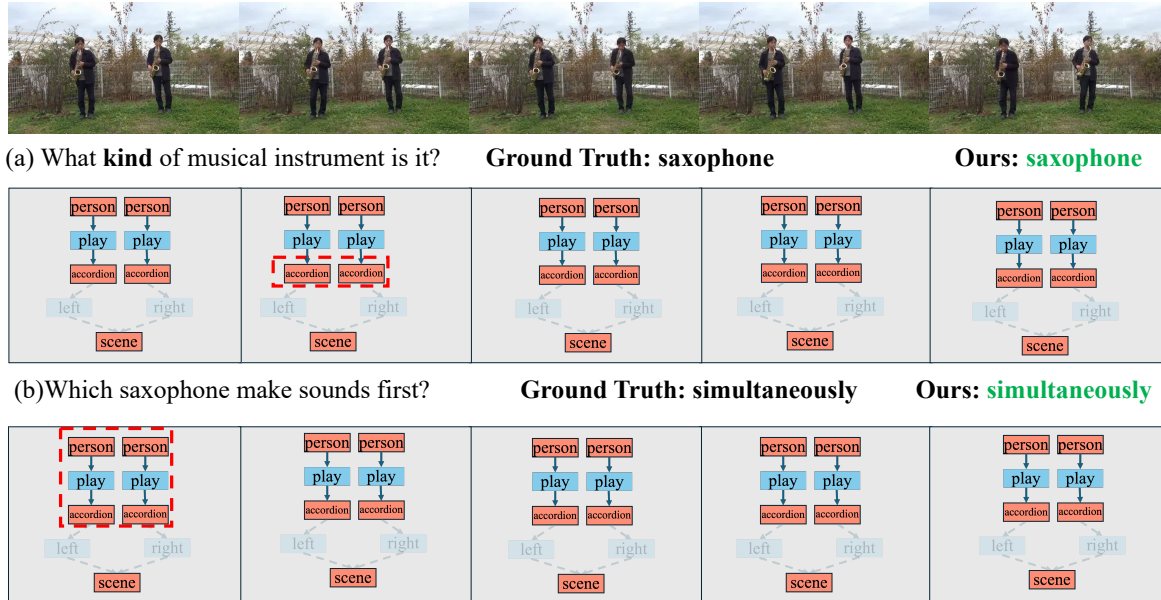


Figure 14. Visualized relationship triplet selection result. In the given example, we convert all the relationship triplets into a scene graph and highlight the triplets selected by our method.